Preprint
UCRL-JC-137615

Effect of Extrusion Temperatures on the Microstructural Development of a Powder Metallurgy Ti-47Al-2Cr-1Nb-1Ta Alloy

L.M. Hsiung, T.G. Nieh

This article was submitted to
9th International Symposium on Processing and Fabrication of Advanced Materials
St. Louis, MO, October 9-12, 2000

June 29, 2000

EFFECT OF EXTRUSION TEMPERATURES ON THE MICROSTRUCTURAL DEVELOPMENT OF A POWDER METALLURGY Ti-47Al-2Cr-1Nb-1Ta ALLOY

L. M. Hsiung and T. G. Nieh

University of California, Lawrence Livermore National Laboratory
Chemistry and Materials Science Directorate
L-369, P.O. Box 808, Livermore, CA 94551-9900

Abstract

Effect of extrusion temperatures on the microstructural development of a powder metallurgy (PM) Ti-47Al-2Cr-1Nb-1Ta (at. %) alloy has been investigated. Microstructure of the PM alloy extruded at 1150 C consists of a fine-grained ($\gamma + \alpha_2$) two-phase structure in association with coarse grains of metastable B2 (ordered bcc) phase. In addition, fine ω (ordered hexagonal) particles are also found within some B2 grains. The PM alloy containing the metastable B2 grains displays a low-temperature superplastic behavior, in which a tensile elongation of 310% is obtained at 800 C under a strain rate of 2×10^{-5} s^{-1}. It is suggested that the decomposition of metastable B2 phase and microstructural evolution during the deformation play a crucial role in the low-temperature superplasticity of the PM TiAl alloy. A refined fully-lamellar (FL) microstructure with alternating γ and α_2 lamellae is developed within the PM alloy extruded at 1400 C. The creep resistance of the refined FL-TiAl alloy is found to be superior to those of the TiAl alloys fabricated by conventional processing techniques. Creep mechanisms for the PM alloy with a refined FL microstructure are critically discussed according to TEM examination of deformation substructure.

Introduction

TiAl-base aluminide alloys are appealing for use in high-temperature structural applications because of their low density, high specific modulus, and good strength retention at elevated-temperatures. However, the inherent poor ductility of titanium aluminides at ambient temperatures has limited their

applications. Alloy design and development to improve their low-temperature ductility, while retaining their strength, have become the major challenge for this alloy system. Alloy and processing developments to improve their low-temperature ductility, while retaining their strength, have become the major challenge [1, 2] for this alloy system. The poor low–temperature ductility causes conventional manufacturing operations such as rolling, forging, drawing, or machining to be difficult for titanium aluminides. Accordingly, the development of superplastic TiAl to produce near-net-shape structural components is technologically attractive. In order to balance low-temperature ductility, fracture toughness and high-temperature mechanical properties of TiAl alloys, recent developments of the alloys have been focused on refining the γ/α_2 lamellar microstructure through advanced processing routes such as powder metallurgy (PM) processes. While both room-temperature and elevated-temperature mechanical properties of PM lamellar TiAl alloy have been demonstrated to be superior to those of the TiAl alloys fabricated by conventional processing techniques, such as ingot metallurgy [3-5], superplastic behavior has recently been observed for the PM alloy containing metastable B2 phase and a fine-grained ($\gamma + \alpha_2$) duplex structure [6]. The results of investigations on the microstructural development within the PM alloy hot extruded at different temperatures as well as the structure-properties relationships are reported here.

Experimental

A titanium aluminide alloy with a nominal composition of Ti-47Al-2Cr-1Nb-1Ta (at.%) was fabricated by a PM process, which involves a hot-extrusion of gas-atomized titanium aluminide powder (particle size: - 200 mesh). The extrusions were carried out at three different temperatures, 1150 C (T_1), 1250 C (T_2) and 1400 C (T_3), which are projected on the Ti-Al phase diagram shown in Fig. 1. The phase content of as-prepared powder and as-fabricated alloy was examined by X-ray diffraction (XRD) using Cu K_α radiation (λ = 0.1546 nm). The detailed microstructures were subsequently examined using transmission electron microscopy (TEM). TEM foils were prepared by a standard twinjet electropolishing technique in an electrolyte of 60% methanol, 35% butyl alcohol, and 5% perchloric acid at ~15 V and -30 C. Test specimens with a gauge dimension of 24.4 x 5.08 x 1.52 mm were fabricated from the annealed materials by electrical discharge machining (EDM). Tensile tests were conducted on alloy samples extruded at T_1 and T2. Tensile tests were conducted at temperatures ranging from 650 to 1100 C, and at strain rates between 10^{-6} and 10^{-4} s^{-1}. A creep test was performed on the alloy samples extruded at T_3 in a dead-load creep machine with a lever arm ratio of 16:1. Creep tests were performed in air in a split furnace with three zones at 760 C and 35 - 400 MPa.

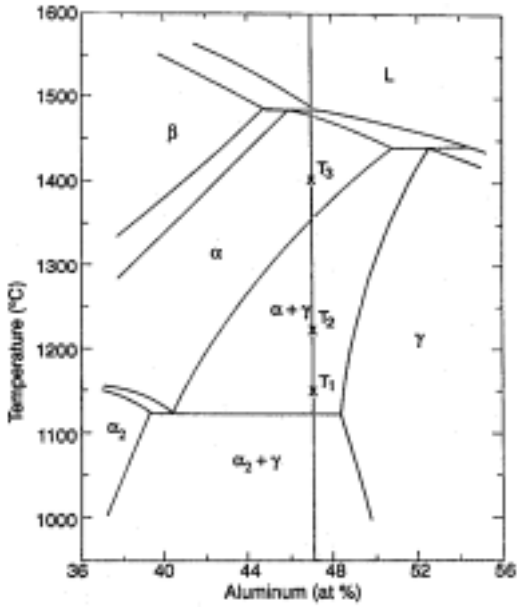

Fig. 1. The extrusion temperatures used to produce typical microstructures, T_1: 1150 °C, T_2: 1250 °C and T_3: 1400 °C, which are projected on the Ti-Al phase diagram.

Results and Discussion

Microstructure of as-prepared powder

An XRD pattern generated from as-prepared powder sample is shown in Fig. 2. It reveals that the powder contains mainly the α phase ($a \cong 0.29$ nm and $c \cong 0.46$ nm) and some supercooled β ($a \cong 0.323$ nm) phases. It is worth noting that the presence of the β phase in titanium aluminide alloys with alloying additions of β stabilizers such as Cr, Mo, and W has been reported previously [7-9]. It is expected that the addition of Ta can further promote the stability of the β phase at low temperatures. Since the microstructures of as-prepared TiAl powder is not in an equilibrium state, the microstructures of PM alloys are anticipated to be sensitive to the processing history. Accordingly, TEM examinations and analyses have been conducted to investigate the effect of processing temperatures on the microstructural development of PM TiAl alloys.

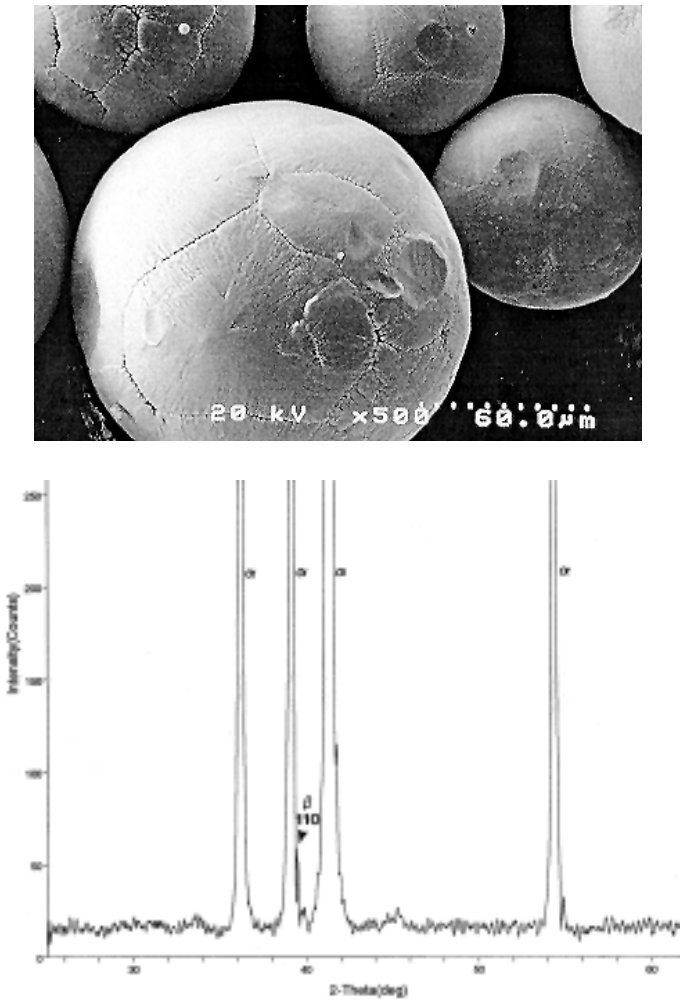

Fig. 2 An XRD pattern (Cu K_α) generated from the as-prepared powder sample.

Microstructural development of PM Ti-47Al-2Cr-1Nb-1Ta

In general, a microstructure consists of coarse B2 (ordered bcc) grains and a fine-grained ($\gamma + \alpha_2$) two-phase structure is obtained within the alloy extruded at 1150 C (near the eutectoid temperature). A microstructure contains coarse

α_2 grains and a fine-grained ($\gamma + \alpha_2$) two-phase structure was formed within the alloy extruded at 1250 °C [in the ($\alpha + \gamma$) phase field]. A lamellar γ/α_2 microstructure was developed within the alloy extruded at 1400 °C (in the α phase field). The details of microstructural development through different extrusion temperatures are demonstrated and discussed below. In addition, the influence of the resulted microstructures on high-temperature mechanical properties (superplasticity and/or creep deformation) of the P/M alloys extruded at T_1 (1150 °C) and T_3 (1400 °C) is also briefly demonstrated.

Microstructure developed at 1150 °C

A typical microstructure of the alloy extruded at 1150 °C is shown in Fig. 3. A distinct microstructure can be found in the different regions of the micrograph shown in Fig. 3 (left). According to electron diffraction analyses, the coarse grains (2 - 5 μm) in the left region are mainly of B2 (ordered bcc) structure, and the fine grains (0.5 - 1 μm) in the right region are a mixture of the γ and α_2 grains. That is, whilst some supercooled β (or B2) grains still remain in the alloy, a two-phase structure composed of equiaxed γ ($L1_0$, TiAl) and α_2 (DO19, Ti_3Al) grains is formed via the $\alpha \rightarrow \gamma + \alpha_2$ transition. Notice that thermal twins are often formed within the γ grains. In addition, elongated grains of supercooled B2 phase is also observed and shown in Fig. 3 (right). Figure 4 is a dark-field TEM image showing the identification of B2 phase. Here, a network of thermal anti-phase boundaries (APBs) observed from a B2 grain [imaged by a superlattice reflection ($\boldsymbol{g}$ = 100) under two-beam conditions] is shown in Fig. 4 (a). The $[001]_{B2}$- and $[111]_{B2}$-zone diffraction patterns of the B2 phase are shown in Fig. 4(b) and 4(c).

In addition to the supercooled B2 phase, fine particles of ordered ω phase ($B8_2$, ordered hexagonal) were also found within some B2 grains. A typical example is shown in Fig. 5. Figure 5(b) is a dark-field image showing the formation of ordered ω particles within a B2 grain shown in Fig. 5(a). The orientation relationships between ordered ω and B2 phases are determined to be $(0001)_\omega \| \{111\}_{B2}$ and $[11\bar{2}0]_\omega \| <1\bar{1}0>_{B2}$ according to the diffraction patterns shown in Fig. 6. The lattice parameters of ordered ω can be derived from that of the parent B2 phase, i.e. $a_\omega = \sqrt{2}\, a_{B2} = 0.457$ nm, and $c_\omega = 3\,(d_{111})_{B2} = 0.559$ nm. It is worth noting that the mechanisms of B2 $\rightarrow$ ordered ω transition have been systematically studied in Ti_3Al+Nb alloys [10,11]. It is proposed that the ordered ω-lattice can be obtained by collapsing one pair of (111) planes within the B2-lattice, and leaving the adjacent (111) planes unaltered as schematically illustrated in Fig. 7.

The results of the alloy samples tensile tested at 800 and 1000 °C are shown in Fig. 8. The total elongation of both samples over 300% was

obtained. Deformation substructure observed from the fractured sample after tested at 800 °C to a 310% elongation is shown in Fig. 9. The observation of dislocation emission near a grain triple junction implies the occurrence of grain boundary sliding during deformation. While the detailed mechanisms for the superplastic behavior of the alloy have been studied and proposed elsewhere [6], we suggest here that the decomposition of metastable B2 phase and microstructural evolution during the deformation play a crucial role in the superplasticity of the PM alloy. The decomposition of B2 phase into fine-grained γ and α_2 phases promotes grain boundary sliding and accommodates the sliding strains to reduce the propensity of cavitation at grain triple junctions and thus delay that fracture process.

(a)

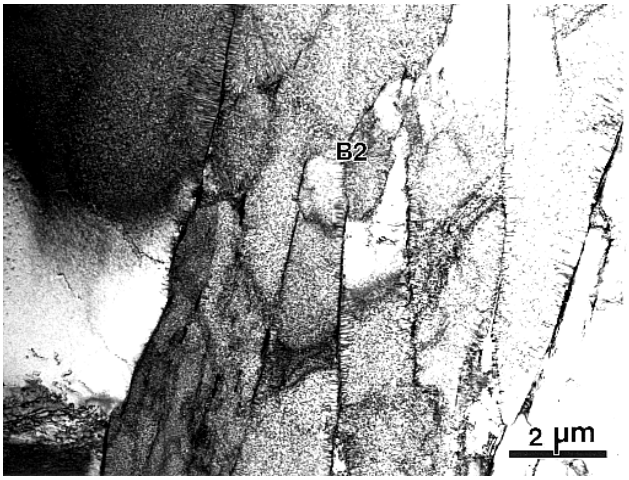

(b)

Fig. 3. TEM images showing typical microstructures of the PM alloy extruded at 1150 °C. (a) Coexistence of coarse B2 grains with fine-grained ($\gamma+\alpha_2$) structure. (b) Elongated B2 grains.

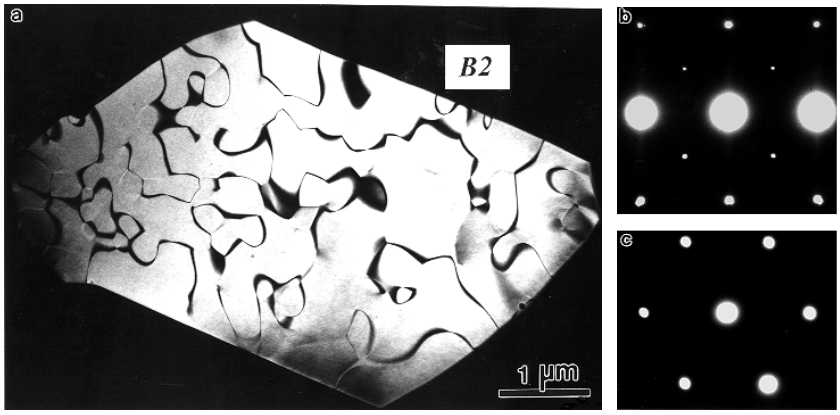

Fig. 4. (a) A dark-field TEM image showing a network of thermal anti-phase boundaries within a B2 grain, and SAD patterns of (b) $[001]_{B2}$-zone, and (c) $[111]_{B2}$-zone.

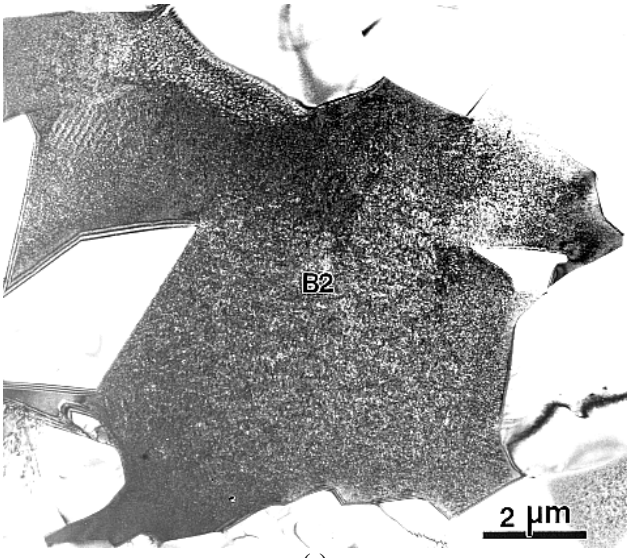

(a)

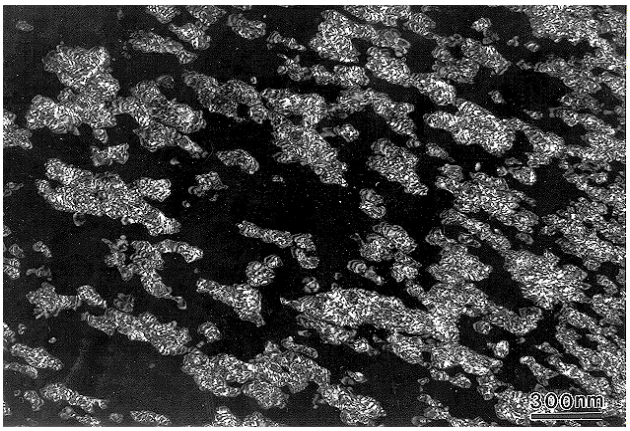

(b)

Fig. 5. A dark-field TEM image showing the formation of ordered ω particles (b) within a B2 grain (a).

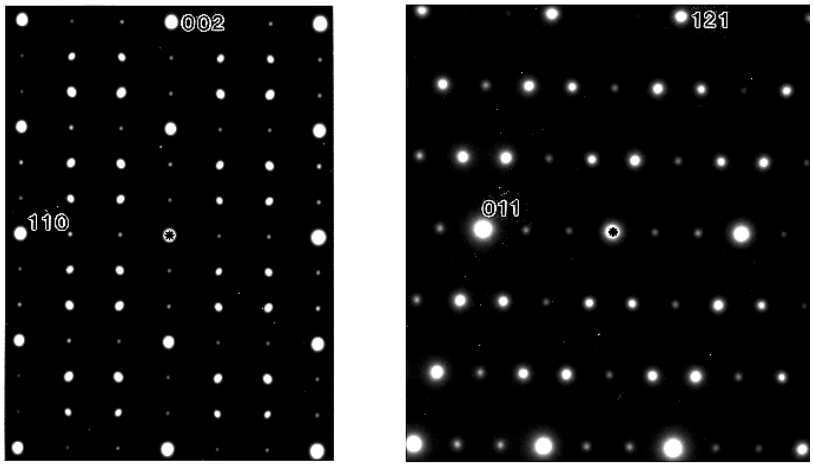

Fig. 6. . Diffraction patterns generated fro two major zone axes of B2 matrix revealing the phase relationships between B2 and ordered ω phase, (left) $[\bar{2}\,110]_{\omega}$ || $<110>_{B2}$, and (right) $[1\bar{2}\,11]_{\omega}$||$<311>_{B2}$.

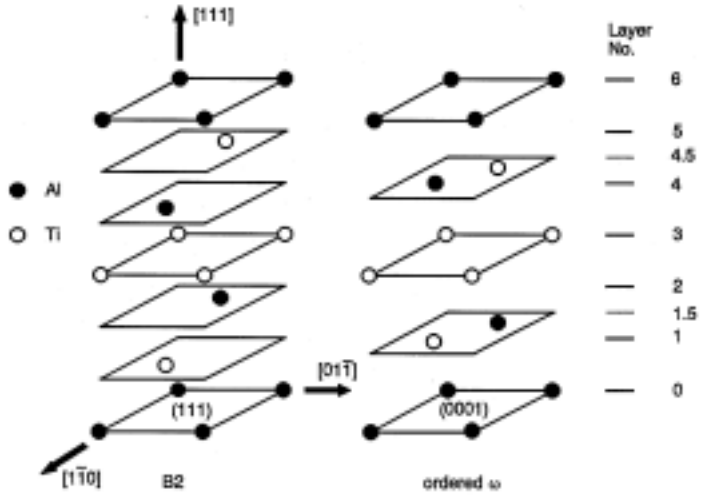

Fig. 7. Lattice correspondence between B2 (ordered bcc) and ordered ω phases based upon the (111)-plane collapse model. The ω-lattice can be obtained by collapsing one pair of (111) planes within B2-lattice.

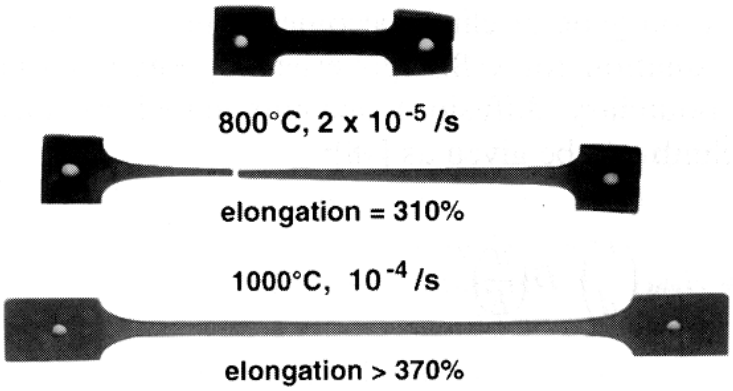

Fig. 8. P/M TiAl samples superplastically deformed at 800° C (middle) and 1000 C (bottom). An as-prepared test piece (top) is also shown for comparison.

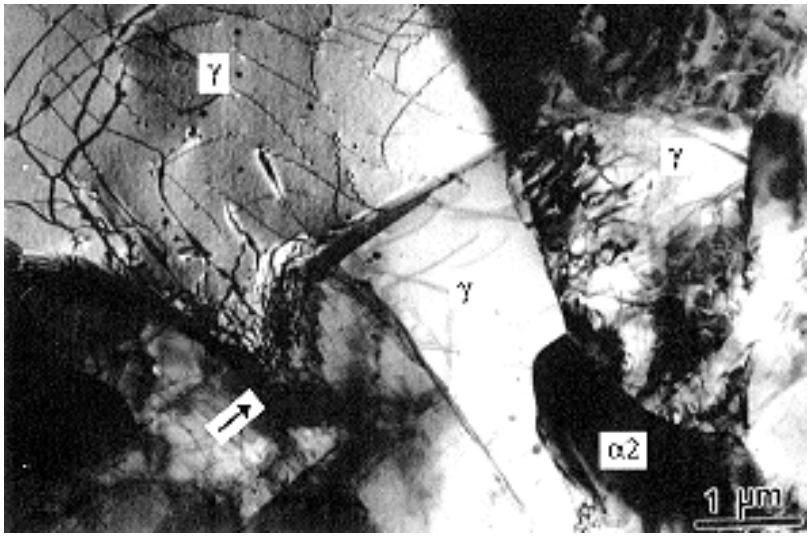

Fig. 9. A coarse two-phase microstructure developed in the sample deformed at 800 C to a fracture (310% elongation). The dislocation emission at a grain-boundary junction (marked by an arrow) suggests that a local stress concentration at junctions causes the sample to fracture.

Microstructure developed at 1250° C

A typical microstructure observed in the alloy extruded at 1250° C is shown in Fig. 9. Similar to that in the alloy extruded at 1150° C, the microstructure contains a two-phase structure of fine γ and α_2 grains [right region of Fig. 9(a)] and coarse α_2 grains [left region of Fig. 9(a)]. Figure 9(b) is a dark-field image showing a network of thermal anti-phase boundaries associated with many planar defects within an α_2-grain. In fact, the planar defects are composed of stacking faults of the α_2 phase and thin plates of γ phase. These can be revealed from a TEM analysis shown in Figs. 9(c) and 9(d). Figure 9(c) is a dark-field TEM image showing some of the planar defects are actually γ plates (5~10 nm thick). A twin relationship among these thin γ plates can also be found from the SAD pattern shown in Fig. 9(d). The orientation relationships between γ and α_2 phases are $(111)_\gamma \parallel (0001)_{\alpha 2}$ and $[110]_\gamma \parallel [11\bar{2}0]_{\alpha 2}$. Similar to the hcp → fcc transformation observed in cobalt [12], the stacking faults are intimately related to the formation of the γ plates within the α_2 grains. It is anticipated that if the transformation further proceeds, γ plates would thicken at the expense of the α_2 phase and eventually a lamellar structure composed of alternating γ and α_2 plates could be formed within the parent α_2 grain. It is worth noting that a tensile elongation of 260% at 1000° C was obtained for the alloy, which is significant inferior to the alloy extruded at 1150° C. This result further supports that the superplastic behavior observed from the alloy extruded at 1150° C is mainly because of the metastable B2 phase formed in the alloy.

(a)

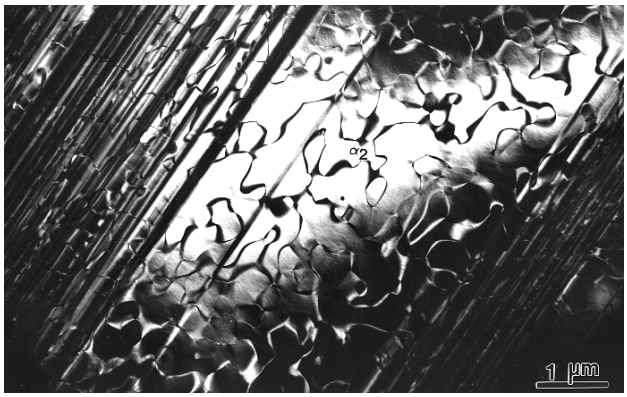

(b)

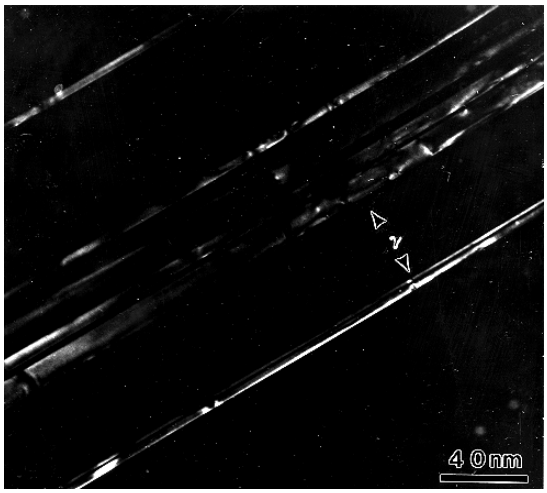

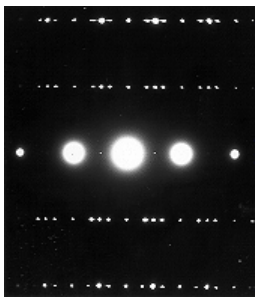

(c) (d)

Fig. 9. (a) A typical microstructure of the alloy extruded at 1250 °C., (b) a dark-field TEM image showing a network of thermal anti-phase boundaries associated with planar defects within an α_2 grain, and (c) a dark-field TEM image revealing that some of the planar defects are γ plates (d) SAD pattern generated from the area in (b), $\mathbf{Z} = [13\bar{2}]_{\gamma} \| [5\bar{4}\,\bar{1}\,0]_{\alpha^2}$.

Microstructure developed at 1400° C

A refined fully-lamellar (FL) structure consisting of alternating lamellae of γ and α_2 phase is developed within the alloy extruded at 1400° C. A typical lamellar structure is shown in Fig. 10(a). The average lamellar grain size is ~60 nm, the lamellar interface spacing varies between 100 nm and 350 nm, and the thickness of α_2 lamellae varies between 10 nm and 50 nm [Fig. 10(b)]. These values are considerably finer than those in the TiAl alloys fabricated by conventional processing techniques [13]. In general, the FL-TiAl contains two types of lamellar interfaces [14]: (1) The γ/α_2 interphase interface which has a usual orientation relationship: $(0001)_{\alpha 2} \parallel (111)_\gamma$ and $<11\bar{2}0>_{\alpha 2} \parallel <1\bar{1}0>_\gamma$ [which can be determined from the SAD pattern shown in Fig. 10(c)]. (2) The γ/γ twin-related interface. Both lattice dislocations within γ lamellae and a high density of interfacial dislocations on inclined lamellar interfaces have been observed in FL-TiAl [15]. While the interfacial dislocations on semi-coherent γ/α_2 interfaces are *1/6*<112> or *1/3*<112> type misfit dislocations, those on γ/γ twin-related interfaces are *1/6*$[11\bar{2}]$ type twinning dislocations or geometry necessary dislocations for accommodating the departure of true-twin interface from the exact (111) twin plane.

Creep data of the PM FL-TiAl alloy tested at 760° C is shown in Fig. 11(a) with a comparison of the creep data of other TiAl alloys reported in literature. It can be clearly seen that there exist two creep regimes for the PM alloy, i.e. the regimes of low stress (*LS*) and high stress (*HS*), and the PM alloy demonstrates the best creep resistance among all in the *HS* regime (> 300 MPa) and relatively better creep resistance in the *LS* regime (< 300 MPa).

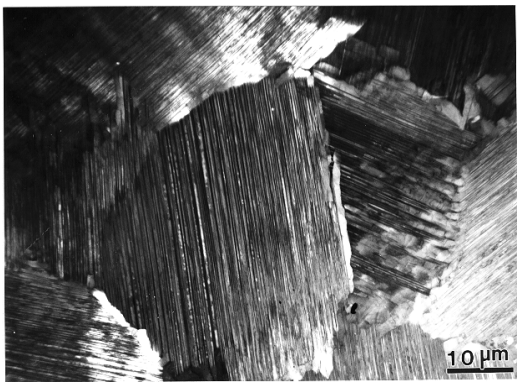

(a)

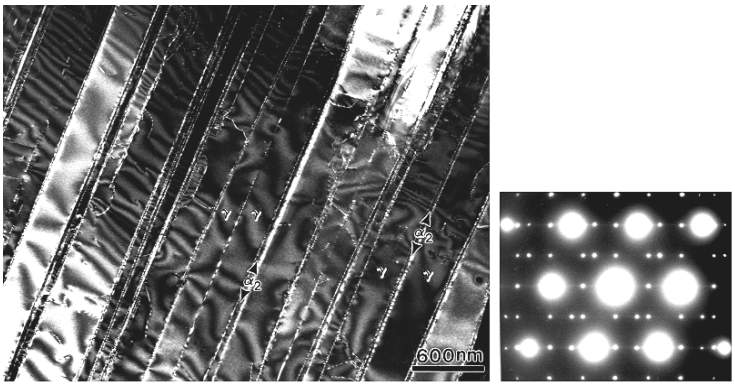

(b) (c)

Fig. 10. (a) A typical microstructure observed from the alloy extruded at 1400 °C, (b) a dark-field TEM image showing an edge-on view of γ/α_2 lamellar microstructure, and (c) an SAD pattern generated from (b) showing the phase relationships between γ and α_2, $\mathbf{Z} = [0\bar{1}1]_\gamma \parallel [01\bar{1}0]_{\alpha 2}$.

Since for real applications the structural components are mainly operated in *LS* regime, we have conduct investigations to understand creep mechanisms in *LS* regime so that the creep resistance of the alloy in *LS* regime can be further improved. Detailed mechanisms based upon the sliding of lamellar interfaces have been recently proposed elsewhere [16]. The evidence of interface sliding caused by the motion of interfacial dislocations during creep at 760 °C and 138 MPa is shown in Figs. 11(b) and 11(c). In general, the high population of interfacial dislocations on lamellar interfaces can act as preferential sites for solute (impurity) segregation. These solutes subsequently can act as short-range barriers for the motion of interfacial dislocations and resulting in the viscous glide of interfacial dislocations in *LS* regime. The zigzag motion of interfacial dislocations presumably caused by locking-unlocking of dislocation lines from solute atoms can be clearly seen in Fig. 11(b). Consequently, grain boundary steps (marked by arrows) were formed as a result of the interface sliding caused by the interfacial dislocation motion [Figure 11 (c)]. These observations suggest that interface sliding is the predominant deformation mode in *LS* regime. Creep resistance in the regime can be promoted by reducing the mobility of interfacial dislocations, which may be achieved by the addition of alloy elements such as W (to reduce diffusivity) or B (to form boride particles at interfaces) to impede the motion of interfacial dislocations.

Summary and Conclusion

The effect of processing temperatures on the microstructural development of a powder metallurgy Ti-47Al-2Cr-1Nb-1Ta (at. %) alloy has been investigated using transmission electron microscopy (TEM) techniques. The as-prepared powder consists of mainly α phase and supercooled β phase. The alloy extruded at 1150 °C is composed of coarse B2 grains and a fine-grained (γ + α_2) two-phase microstructure. Ordered ω particles are also found to form within some B2 grains. The orientation relationships between ordered ω and B2 phases are determined to be $(0001)_\omega \| \{111\}_{B2}$ and $[11\bar{2}0]_\omega \| <1\bar{1}0>_{B2}$, and the lattice parameters of ordered ω are a_ω = 0.457 nm, and c_ω = 0.559 nm. The alloy containing the metastable B2 grains displays a low-temperature superplastic behavior, in which tensile elongations of over 300% is obtained at 800 °C. The alloy extruded at 1250 °C is composed of coarse α_2 grains and a fine-grained (γ + α_2) two-phase microstructure. The observation of stacking faults coexisted with thin γ plates within the α_2 grains reveals that the stacking faults are intimately related to the formation of lamellar microstructure with alternating γ and α_2 lamellae. A refined fully-lamellar (FL) microstructure (γ lamellae: 100 ~ 300 nm thick, and α_2 lamellae: 10 ~ 50 nm thick) is developed for the alloy extruded at 1400 °C. The creep resistance of the refined FL-TiAl alloy is found to be superior to those of the TiAl alloys fabricated by conventional processing techniques.

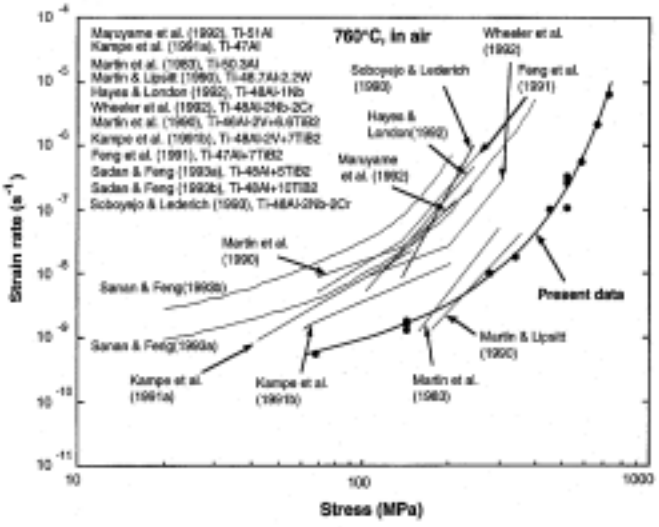

(a)

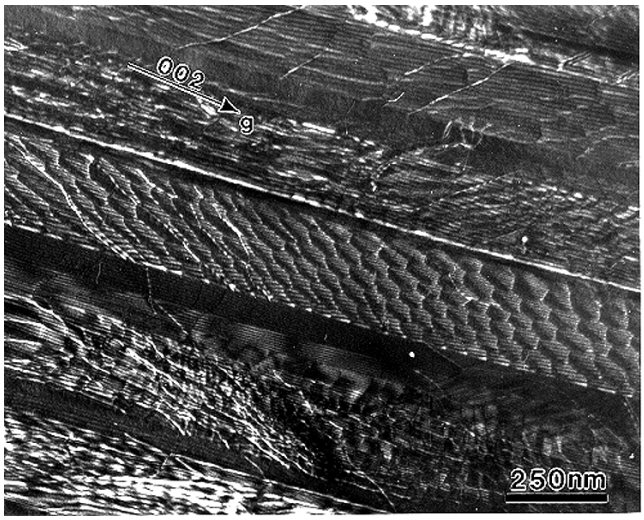

(b)

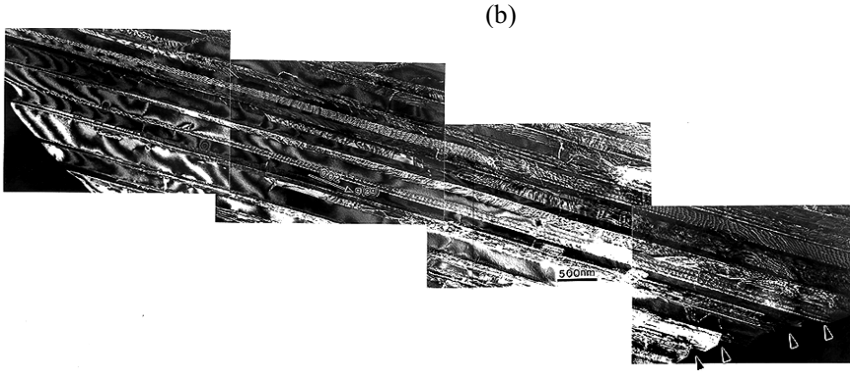

(c)

Fig. 11. (a) A comparison of the creep resistance at 760° C between the presently studied PM alloy and other TiAl alloys [3]. (b) A weak-beam TEM image shows the zigzag motion of interfacial dislocation array in a specimen crept at 760° C with constant loading of 136 MPa. (c) A TEM image shows the formation of grain boundary ledges (marked by arrows) as a result of interfacial sliding caused by the motion of interfacial dislocations.

Acknowledgments

This work was performed under the auspices of the U.S. Department of Energy through contract # W-7405-Eng-48 with Lawrence Livermore National Laboratory. The authors would like to express their gratefulness to Dr. C. T. Liu of Oak Ridge National Laboratory for providing PM TiAl alloys used for this study.

References

1. Y-W. Kim and D.M. Dimiduk, *JOM*, **43**(8), 40 (1991).
2. M. Yamaguchi, *Mater. Sci. Technol.*, **8,** 299 (1992).
3. J.N. Wang, A.J. Schwartz, T.G. Nieh, C.T. Liu, V.K. Sikka and D. Clemens, in *Gamma Titanium Aluminides*, ed. Y-W. Kim et al., TMS, Warrendale, 949 (1995).
4. C.T. Liu, P. J. Maziasz, D.R. Clemens, J.H. Schneibel, V.K. Sikka, T.G. Nieh, J. Wright, and L.R. Walker, in *Gamma Titanium Aluminides*, ed. Y-W. Kim et al., TMS, Warrendale, 679 (1995).
5. C. T. Liu, J.H. Schneibel, P. J. Maziasz, J. L. Wright and D.S. Easton, *Intermetallics*, **4**, 429 (1996).
6. T. G. Nieh, L. M. Hsiung and J. Wadsworth, *Intermetallics*, **7**, 163 (1999).
7. M. A. Morris, Y. G. Liand and M. Leboeuf, *Scripta Metall. Mater*., **31**, 449 (1994).
8. K. Nakai, T. Ono, H. Ohtsubo and Y. Ohmoni, *Mater. Sci. Engng*., **192/193A**, 922 (1995).
9. N. Masahashi and Y. Mizuhara, in *Gamma Titanium Aluminides*, ed. Y-W. Kim et al., TMS, Warrendale, 165 (1995).
10. R. Strychor, J.C. Williams and W.A. Soffa, Met. Trans. A., **19A**, 225 (1988).
11. L. A. Bendersky, W. J. Boettinger, B. P. Burton and F. S. Biancaniello, *Acta Metall. Mater*., **38**, 931 (1990).
12. J. A. Graves, L. A. Bendersky, F.S. Biancaniello, J.H. Perepezko and W. J. Boettinger, *Mater. Sci. Engng*., **98**, 265 (1988).
13. Y-W. Kim, *Mater. Sci. Engng*, **192A**, 519 (1995).
14. M. Yamaguchi and Y. Umakoshi, *Progress in Materials Science*, **34**, 1 (1990).

15. L. M. Hsiung and T. G. Nieh, *Mater. Sci. Engrg*., **A239-240**, 438 (1997).
16. L. M. Hsiung and T. G. Nieh, *Intermetallics*, **7**, 821 (1999).